Analytical Models for Predicting Penetration Depth During Slot Die Coating onto Porous Media

Xiaoyu Ding
School of Mechanical Engineering, Beijing Institute of Technology, Beijing 100081, China

G. W. Woodruff School of Mechanical Engineering, Georgia Institute of Technology, Atlanta, GA 30332

Joshua Prince Ebin and Tequila A.L. Harris
G. W. Woodruff School of Mechanical Engineering, Georgia Institute of Technology, Atlanta, GA 30332

Zhuo Li
School of Materials Science and Engineering, Georgia Institute of Technology, Atlanta, GA 30332

Thomas F. Fuller
School of Chemical & Biomolecular Engineering, Georgia Institute of Technology, Atlanta, GA 30332

DOI 10.1002/aic.14570
Published online August 12, 2014 in Wiley Online Library (wileyonlinelibrary.com)

A series of analytical models have been developed to predict the penetration depth during slot die coating on porous media. Analytical models for both Newtonian and non-Newtonian fluids were derived based on Lubrication Theory, Darcy's law, and a modified Blake–Kozeny equation. Using these models, the penetration depth can be quickly solved and the effects of material properties and processing conditions on penetration depth can be easily investigated. Experiments of coating Newtonian glycerin and non-Newtonian blackstrap molasses onto Toray series carbon paper were conducted to validate developed models. The overall relative error between the predicted and measured penetration depth was found to be typically lower than 20%, which demonstrates the relative accuracy of developed models. Furthermore, based on a parametric study, it was found that the effect of capillary pressure on penetration depth is less than 10% when the ratio of coating bead pressure and capillary pressure is larger than 10. © 2014 American Institute of Chemical Engineers *AIChE J*, 60: 4241–4252, 2014
Keywords: porous media, slot die coating, penetration

Introduction

Coating porous media plays an important role in providing functional properties for composite materials, of which there are many examples. Phase-change materials or silicon–carbide coatings provide thermal insulation for sporting clothes to maintain a suitable temperature for the human body.[1] Polyurethanes coatings are used to add a breathable waterproof property for clothes.[2] A back coating such as an acrylic resin loaded with ammonium polyphosphate has been shown to improve the fire-retardant properties of textiles.[3] Conductive-polymer coatings, such as poly(3,4-ethylenedioxythiophene), have been used to produce electro-active fabrics.[4] In addition to the applications in this article and textile industries, coating porous media also has broad applications in other fields such as the energy sector to fabricate functional multilayer structures. Recently, directly coating polymer electrolyte membrane (PEM) on porous catalyzed gas diffusion layer has been used to manufacture the membrane electrolyte assembly for PEM fuel cells.[5,6]

A major concern when coating porous media is fluid penetration into the substrate. Although some level of penetration is desirable to obtain specific material properties, inadequate or excessive fluid penetration can negatively affect the strength,[7] appearance,[8] functionality, and performance[9] of the resulting material. It has been shown that excessive penetration of Nafion® into the catalyzed gas-diffusion layer during direct coating can reduce the performance of the fuel cell due to poor gas transport and an imbalance between ionic conductivity and electronic conductivity.[5,6]

Modeling work has been conducted for predicting and controlling the penetration depth during direct coating on porous media.[7,10–13] However, a major technical issue that remains is how to determine the pressure in the coating bead. In order to simplify the modeling procedure, some researchers decoupled the flows in the porous media and coating bead, and used approximate pressure distributions in the modeling of penetration. Letzelter and Eklund[10] used a piecewise constant pressure to approximately study the penetration during blade coating on paper. Yesilalan et al.[7] used the pressure distribution on a solid substrate to approximately predict the maximum possible penetration depth during blade coating on a woven fabric. Decoupling the flows in the porous media and coating bead can simplify the model, but introduces error because the flow in the coating

Correspondence concerning this article should be addressed to T. A. L. Harris at tequila.harris@me.gatech.edu.

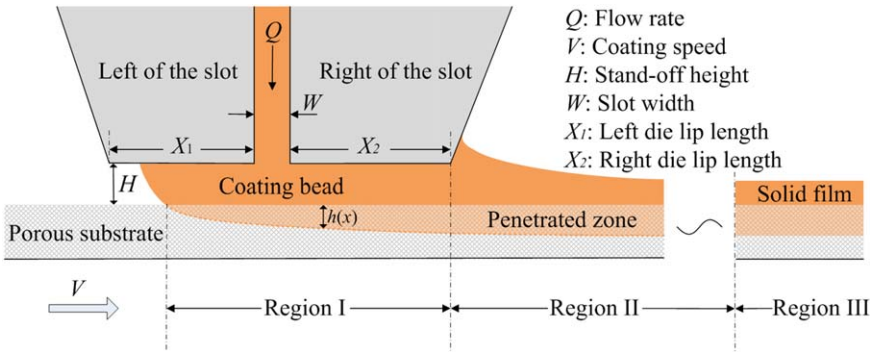

Figure 1. Schematic illustrating the slot die coating on a porous substrate.

[Color figure can be viewed in the online issue, which is available at wileyonlinelibrary.com.]

bead and the flow in the porous media are physically coupled at the interface, and the pressure in the coating bead will be affected by the penetration in the porous media. To improve the accuracy, work has been conducted to couple the two flows to obtain a more precise pressure distribution. Chen and Scriven[11] studied the penetration into a porous substrate for a flooded-nip-blade coating process. In their model, the pressure distribution and penetration depth are calculated simultaneously using a modified lubrication theory. Ninness et al.[12] as well as Devisetti and Bousfield[13] used a similar method to study the penetration into the porous substrates during roll coating. Although these models agree well with the flow dynamics, complex mathematical iterations are required to solve for the penetration depth. Therefore, these models fail to provide clear analytical relationships between coating parameters and the penetration depth. In addition, these models are only applicable for Newtonian fluids.

In order to overcome the drawbacks of above modeling approaches, Ding et al.[14] developed analytical models to predict the penetration depth during slot die coating on porous substrates, for Newtonian and non-Newtonian fluids. However, the predictions only qualitatively followed the same trend as their preliminary experimental results because the capillary pressure in the porous media was ignored in these models, which can have a significant effect on fluid penetration for given coating conditions.

In this article, a series of analytical models are developed to predict the penetration depth during slot die coating accounting for the effect of capillary pressure in the porous media, for Newtonian and non-Newtonian fluids. Lubrication equations,[15] Darcy's law, and a modified Blake–Kozeny equation[16,17] are used to provide simple expressions for calculating the final penetration depth of a fluid into a porous domain. In addition, a dimensionless parameter is established to evaluate the effect of capillary pressure on penetration depth. Experiments of coating Newtonian glycerin and non-Newtonian blackstrap molasses onto Toray series carbon paper are conducted and the values of penetration depth are measured.

Analytical Models of Penetration Depth

Modeling domain and assumptions

A localized scheme of slot die coating on a porous substrate is shown in Figure 1. The coated fluid is delivered through a fixed slot, W, onto a moving substrate to form a coated film. In Figure 1, Q is the flow rate; V is the speed of the substrate (coating speed); and H is the distance between the slot die and the substrate (stand-off height). A coating bead is formed between the slot die and the substrate, and the fluid partially penetrates into the substrate under the coating bead. As shown in Figure 1, the penetration depth, $h(x)$, increases gradually from a point in the left channel to the right outlet of the slot-die. As discussed by Ding et al.,[14] fluid penetration under the slot die lip (Region I in Figure 1) is mainly governed by the pressure in the coating bead and the capillary pressure in the porous media. The fluid properties in this region can be taken as constant, because the residence time of the fluid suspended on the substrate in this region can be as short as a few milliseconds.[18] Fluid penetration after passing the right slot die lip (Region II in Figure 1) is mostly governed by capillary pressure in the porous media. In this region, the coated fluid undergoes a phase transition from liquid to solid. Due to the uncertainty of material properties during the phase transition process, it is very difficult to model the penetration beyond the slot die. However, if the coated fluid is highly viscous, and if the capillary force is relatively small, the penetration changes during the phase transition process will be relatively small. Consequently, most studies consider only the penetration under the slot die lips or the coating bead,[7,10–13,18–20] which will be a similar approach used in this work.

The capillary pressure can either aid or hinder fluid penetration into porous media depending on the hydrophobicity or hydrophilicity of the fluid, which is a function of the contact angle. If the contact angle is lower than 90°, the capillary pressure is expected to pull the fluid into the porous media, since it will have a hydrophilic nature. Otherwise, the fluid will be repelled because of its hydrophobic nature. However, both the contact angle and capillary pressure within porous media will change with time, and determining their respective values can be complex.[21–23] In this study, the capillary pressure is calculated with the Young–Laplace equation

$$p_c = \frac{2\sigma \cos\theta}{r} \tag{1}$$

where σ is surface tension, θ is contact angle of coating liquid on the surface of porous media, and r is the average pore radius. It can be seen that the capillary pressure is a constant positive value when it absorbs the fluid into the

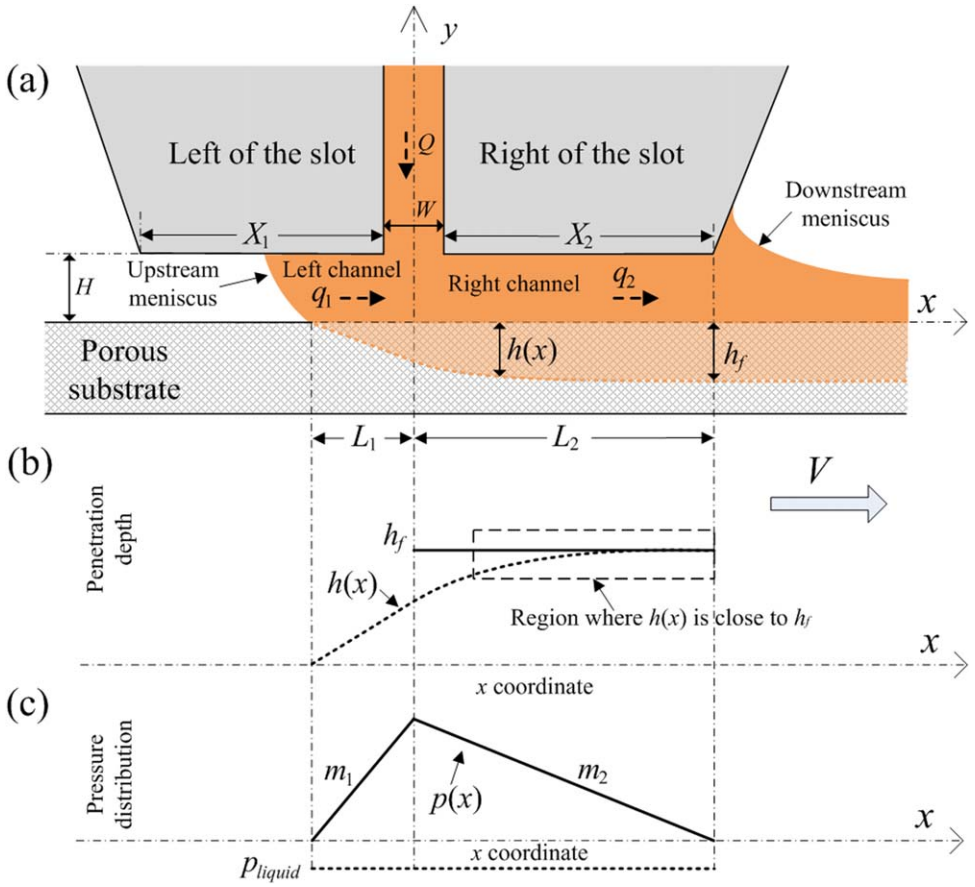

Figure 2. Schematic of (a) the slot die configuration, (b) analytical penetration, and (c) pressure distribution with a positive capillary pressure.

[Color figure can be viewed in the online issue, which is available at wileyonlinelibrary.com.]

porous media (hydrophilic or contact angle <90°); or a negative value when it pushes fluid out of the porous media (hydrophobic or contact angle >90°).

Nomenclature found in Figures 1–3 is used for the derivation of the analytical models of penetration depth. The derivation is based on the schematic of flow field in Figures 2 and 3 and on the following simplifying assumptions:

1. The 1-D modified Blake–Kozeny equation describes fluid flow during coating of a non-Newtonian fluid. For a Newtonian fluid, the Blake–Kozeny equation reduces to Darcy's law.
2. Flow in the coating bead (Region I in Figure 1) is laminar and fully developed.
3. Capillary pressure in the porous media is assumed to be a constant value (zero, positive, or negative); whereas the capillary effect on the upstream and downstream menisci of the coating bead is ignored.
4. Penetration velocity is relatively slow, and the total penetration flow rate is much slower than the total flow rate, Q.
5. The coating is formed at a relatively high coating speed, while the upstream meniscus always stays in the left channel, and the downstream meniscus always stays outside the right outlet.
6. The right channel length, L_2, is much longer than either the slot width, W, or the stand-off height, H.
7. The coating is conducted within the defect-free coating boundary, that is, no air entrainment or pinholes.

Analytical penetration depth for Newtonian fluids with a positive capillary pressure

In this section, a positive capillary pressure is assumed to exist for the two-phase flow in the porous media. The derivation in this section is based on the schematic in Figure 2. Capillary pressure (p_c) is defined as $p_c = p_{air} - p_{liquid}$, where p_{air} is the reference pressure, which is defined as zero. Therefore, $p_{liquid} = -p_c$, where p_{liquid} is the pressure at the front of penetrated fluid. The overall driving pressure for penetration is $p(x) - p_{liquid} = p(x) + p_c$ where $p(x)$ is the pressure in the coating bead. As shown in Figure 2c, when p_c is positive p_{liquid} will be negative. In this case, the overall driving pressure for penetration increases compared to having no capillary pressure. Therefore, the positive capillary pressure is expected to increase the fluid penetration.

Applying Darcy's law, the penetration velocity, $v_p(x)$, along the porous media is given by

$$v_p(x) = \frac{k}{\mu\varepsilon}\frac{dp}{dy} = \frac{k}{\mu\varepsilon}\frac{p(x)+p_c}{h(x)} \tag{2}$$

where k is the permeability, ε is the porosity of the porous media, μ is the viscosity of the coated fluid, and $h(x)$ is the penetration depth along the porous media. $p(x)$ and $h(x)$ are functions of coordinate x, as shown in the Figure 2.

$v_p(x)$ is also be given by

$$v_p(x) = \frac{d[h(x)]}{dt} = \frac{d[h(x)]}{dx}\frac{dx}{dt} = \frac{d[h(x)]}{dx}V \tag{3}$$

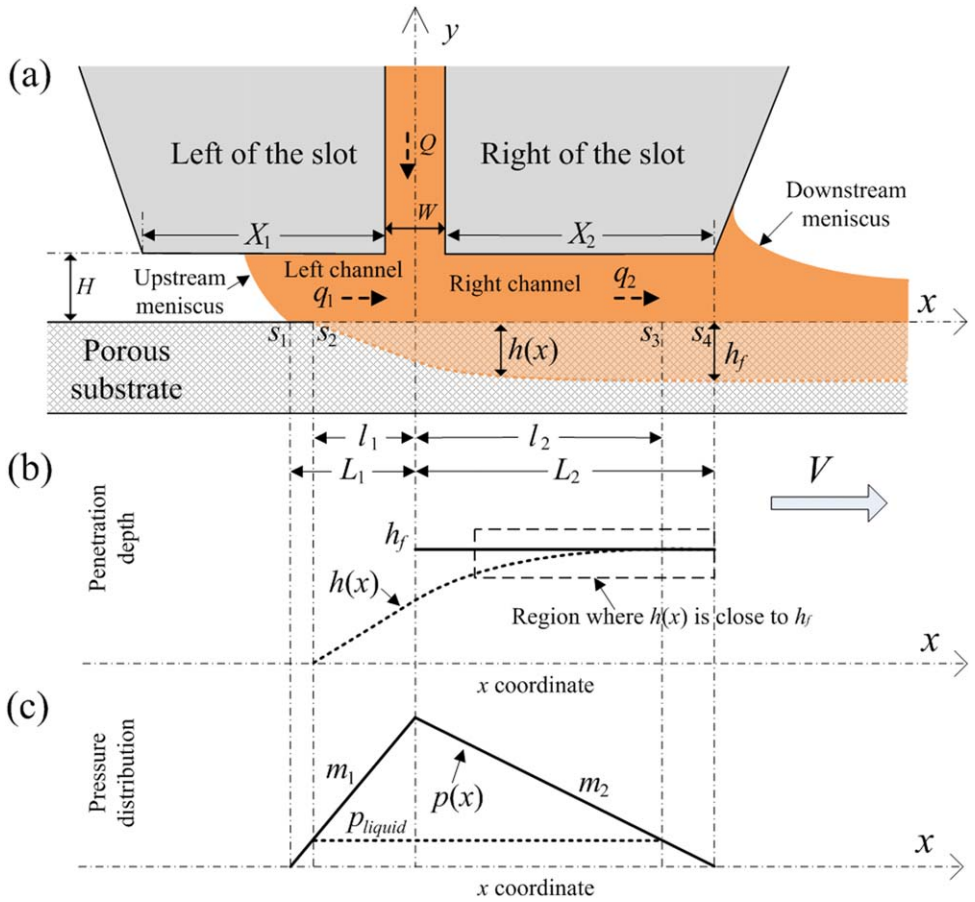

Figure 3. Schematic of (a) the slot die configuration, (b) analytical penetration, and (c) pressure distribution with a negative capillary pressure.

[Color figure can be viewed in the online issue, which is available at wileyonlinelibrary.com.]

Substituting Eq. 3 into Eq. 2 yields

$$h(x)\cdot d[h(x)]=\frac{k}{\mu V\varepsilon}[p(x)+p_c]\cdot dx \tag{4}$$

A modified lubrication theory[12] is applied to determine the pressure gradients (absolute values) m_1 and m_2, in the left and right channels, respectively. Utilization of the modified lubrication theory is justified by Assumptions 2–4. The pressure gradients are given by

$$m_1=\frac{6\mu(VH-2q_1)}{H^3}\quad\text{(left channel)} \tag{5.1}$$

$$m_2=\frac{-6\mu(VH-2q_2)}{H^3}\quad\text{(right channel)} \tag{5.2}$$

Where q_1 and q_2 are the flow rates in the left channel and right channel, respectively. When coating on a solid substrate, q_1 equals zero and q_2 equals the inlet flow rate Q. When coating on a porous substrate, q_1 and q_2 are functions of x due to the effect of penetration. However, if the flow rate of penetration is much smaller than the total flow rate, Q (Assumption 4), q_1 and q_2 can be assumed to be constants. Consequently, m_1 and m_2 can also be assumed to be constants. Thus, the pressure distribution, $p(x)$, in the left channel and right channel, respectively, can be given by

$$p(x)=m_1(L_1+x)\quad(x<0,\text{left channel}) \tag{6.1}$$

$$p(x)=m_2(L_2-x)\quad(x>0,\text{right channel}) \tag{6.2}$$

Substituting Eq. 6.1 into Eq. 4 and integrating from $x=-L_1$ to 0 gives the expression of the penetration depth at $x=0$, h_0, given by

$$h_0=\sqrt{\frac{kL_1}{\mu V\varepsilon}[m_1L_1+2p_c]} \tag{7}$$

Substituting Eq. 6.2 into Eq. 4, integrating from $x=0$ to L_2, and using the mathematical relationship that equates the pressure on both sides of the die, $m_1L_1=m_2L_2$, and using the expression of h_0, gives the final penetration depth at $x=L_2$

$$h_f=\sqrt{\frac{k}{\mu V\varepsilon}\left[m_2L_2{}^2+\frac{m_2{}^2L_2{}^2}{m_1}+2p_cL_2+2p_c\frac{m_2L_2}{m_1}\right]} \tag{8}$$

m_1 and m_2 in Eq. 6.2 are still unknown. As discussed by Ding et al.,[14] m_1 and m_2 can be approximated in the following way. If the coating velocity is relatively high (Assumption 5), which is always desired to increase the production rate in practice, the upstream meniscus will be close to the center slot; that is, L_1 will be relatively small. By assuming a small penetration velocity (Assumption 4), the total penetration in the left channel is negligible. Thus, q_1 can be approximated as zero, similar to the case of coating a solid substrate. In the right channel, since L_2 is much longer than W and H (Assumption 6), and understanding that the change of $h(x)$ gradually diminishes with x, the penetration depth in

most of the right channel is expected to be close to the final penetration depth at the outlet, h_f, as depicted by the dashed box in Figure 2b. Therefore, q_2 can be approximated by the flow rate at the right outlet, which is given by $Q-h_fV\varepsilon$.

Substituting $q_1 \approx 0$ and $q_2 \approx Q-h_fV\varepsilon$ into Eqs. 5.1 and 5.2 gives

$$m_1 \approx \frac{6\mu V}{H^2} \quad \text{(left channel)} \tag{9.1}$$

$$m_2 \approx \frac{-6\mu[VH-2(Q-h_fV\varepsilon)]}{H^3} \quad \text{(right channel)} \tag{9.2}$$

Substituting Eq. 9.1 into Eq. 6.2 and solving Eqs. 6.2 and 9.2 gives an quadratic function for h_f

$$A\times h_f{}^2+B\times h_f+C=0, \tag{10}$$

where

$$A=\frac{24kL_2{}^2\varepsilon}{H^4}-1,$$

$$B=\frac{12kL_2{}^2}{H^4V}\left(VH-4Q-\frac{p_cH^3}{3\mu L_2}\right), \text{and}$$

$$C=\frac{6k(2Q-VH)}{H^4V^2\varepsilon}\left(2QL_2{}^2+\frac{p_cL_2H^3}{3\mu}\right)+\frac{2kp_cL^2}{\mu V\varepsilon}$$

In Eq. 10, A, B, and C are calculated using known coating conditions. As expected, when $p_c=0$, Eq. 10 simplifies to Ding et al.'s[14] earlier model.

Analytical penetration depth for Newtonian fluids with a negative capillary pressure

In this section, a negative capillary pressure is assumed to exist for the two-phase flow in the porous media. The derivation in this section is based on the schematic in Figure 3. As discussed above, $p(x)-p_{liquid}=p(x)+p_c$ is the overall driving pressure for penetration. When p_c is negative p_{liquid} will be positive, as shown in Figure 3c. In this case, the overall driving pressure for penetration is decreased compared with no capillary pressure case. Therefore, the negative capillary pressure is expected to decrease the fluid penetration.

As shown in Figure 3, from the position of dynamic contact line, s_1, to the position, s_2, the pressure in the coating bead, $p(x)$, is smaller than p_{liquid}. Thus, there is no penetration from s_1 to s_2, that is, the penetration starts from s_2. The penetration depth gradually increases from s_2 to s_3. From s_3 to the outlet, s_4, the pressure in the coating bead is smaller than p_{liquid}. Therefore, the penetration depth is expected to decrease from s_3 to s_4, that is, the penetrated fluid will want to draw upward in y, and out of the porous media. However, the real dynamics is more complex. The penetrated fluid does not necessarily decrease due to the effects of the receding contact angle and pinning behavior,[24] which will be discussed in detail later. In this study, the penetration depth from s_3 to s_4 is assumed to be constant. The derivation for the final penetration depth, h_f, with a negative capillary pressure will be limited in the region, s_2–s_3. For this derivation, a similar approach used for the positive capillary pressure is taken.

Substituting Eq. 6.1 into Eq. 4 and integrating from $x=-l_1$ to 0 where l_1 can be calculated by $l_1=L_1+\frac{p_c}{m_1}$, gives the expression of the penetration depth at $x=0$, h_0, given by

$$h_0=\sqrt{\frac{kL_1}{\mu V\varepsilon}\left[m_1L_1{}^2+2p_cL_1+\frac{p_c{}^2}{m_1}\right]} \tag{11}$$

Then, substituting Eq. 6.2 into Eq. 4, integrating from $x=0$ to l_2, where l_2 can be calculated by $l_2=L_2+\frac{p_c}{m_2}$, and using the mathematical relationship that equates the pressure on both sides of the die, $m_1L_1=m_2L_2$, gives the expression of final penetration depth at $x=l_2$

$$h_f=\sqrt{\frac{k}{\mu V\varepsilon}\left[\frac{m_2{}^2L_2{}^2}{m_1}+m_2L_2{}^2+2p_cL_2\left(\frac{m_2}{m_1}+1\right)+\left(\frac{1}{m_1}+\frac{1}{m_2}\right)p_c{}^2\right]} \tag{12}$$

where m_1 and m_2 are given by Eqs. 9.1 and 9.2.

Equation 9.2 is an implicit analytical expression of the final penetration depth because m_2 is a function of h_f. As expected, when $p_c=0$, Eq. 9.2 simplifies to Ding et al.'s[14] earlier model.

Analytical penetration depth for non-Newtonian fluids

For a non-Newtonian fluid, the power law model is usually used to describe its rheological properties, by: $\mu_{app}=m\dot{\gamma}^{n-1}$, where μ_{app} is the apparent viscosity, $\dot{\gamma}$ is the shear rate, m is the consistency index, and n is the flow behavior index. When coating a non-Newtonian fluid, the modified Blake–Kozeny equation is used to calculate the penetration velocity in the porous media, which is given by[16]

$$v_p(x)=\left[\frac{k}{\mu_{eff}}\frac{p(x)+p_c}{h(x)}\right]^{1/n}\frac{1}{\varepsilon} \tag{13}$$

where μ_{eff} is an effective viscosity defined by: $\mu_{eff}=\frac{m}{12}\left(9+\frac{3}{n}\right)^n(150k\varepsilon)^{(1-n)/2}$.

In addition, a generalized lubrication theory for non-Newtonian fluids derived by Dien and Elrod[15] is used to calculate the absolute values of the pressure gradients in the left and right channels, which are given by

$$m_3=\frac{6\bar{\mu}(VH-2q_1)}{H^3} \quad \text{(left channel)} \tag{14.1}$$

$$m_4=\frac{-6\bar{\mu}(VH-2q_2)}{H^3} \quad \text{(right channel)} \tag{14.2}$$

where $\bar{\mu}\equiv mn\left(\frac{V}{H}\right)^{n-1}$. It has been demonstrated that Eqs. 14.1 and 14.2 give relatively good approximations for the pressure gradient when the flow behavior index, n, is higher than 0.5 and the flow rate in the channel is between $0.2VH$ and $0.8VH$.[15]

Substituting $q_1 \approx 0$ and $q_2 \approx Q-h_fV\varepsilon$ into Eqs. 14.1 and 14.2 gives

$$m_3 \approx \frac{6\bar{\mu}V}{H^2} \quad \text{(left channel)} \tag{15.1}$$

$$m_4 \approx \frac{-6\bar{\mu}[VH-2(Q-h_fV\varepsilon)]}{H^3} \quad \text{(right channel)} \tag{15.2}$$

For coating non-Newtonian fluids, Eq. 13 replaces Eq. 2 as the momentum equation, whereas Eq. 3 is still used to account for mass conservation. Substituting Eq. 3 into Eq. 13 yields

$$[h(x)]^{1/n}\cdot d[h(x)]=\left[\frac{k[p(x)+p_c]}{\mu_{eff}}\right]^{1/n}\frac{1}{V\varepsilon}\cdot dx \tag{16}$$

Table 1. Properties of Different Porous Media with Respect to Molasses and Glycerin as Applicable

Substrate	Permeability k (m^2)	Porosity ε	Average pore radius r (μm)	Contact angle θ (°)		Capillary pressure p_c (Pa)	
				Molasses	Glycerin	Molasses	Glycerin
Toray 090 (batch 1)	8.99×10^{-1229}	0.79[29]	9.5[30]	98.9 ± 7.5	99.5 ± 6.5	−1500	−2200
Toray 090 (batch 2)	8.99×10^{-1229}	0.79[29]	9.5[30]	122.9 ± 10.2	115.9 ± 5.0	−5400	−5800
Toray 090 (PTFE)	6.36×10^{-1231}	0.69[31]	8.5[32]	146.6 ± 4.2		−9200	

Then, following the similar derivation procedure used for Newtonian fluids, the analytical models of penetration depth for non-Newtonian fluids are obtained. Specifically, for a positive capillary pressure, the expression of final penetration depth at $x=L_2$, h_f, is given by

$$h_f^{(n+1)/n}=\left(\frac{k}{\mu_{eff}}\right)^{1/n}\frac{1}{V\varepsilon}\left(\frac{1}{m_3}+\frac{1}{m_4}\right)\left[(m_4L_2+p_c)^{(n+1)/n}-p_c^{(n+1)/n}\right] \quad (17)$$

For a negative capillary pressure, the expression of final penetration depth at $x=l_2$, h_f, is given by

$$h_f^{(n+1)/n}=\left(\frac{k}{\mu_{eff}}\right)^{1/n}\frac{1}{V\varepsilon}\left(\frac{1}{m_3}+\frac{1}{m_4}\right)(m_4L_2+p_c)^{(n+1)/n} \quad (18)$$

In Eqs. 14.1 and 14.2, m_3 and m_4 are calculated by Eqs. 15.1 and 15.2, respectively. Equations 14.1 and 14.2 are implicit analytical expressions of the final penetration depth, because m_4 is a function of h_f. As expected, when $p_c=0$, Eqs. 14.1 and 14.2 will generate the same form as Ding et al.'s[14] model.

Determination of the physically correct penetration depth

Equation 10 above has a standard quadratic form, which can be solved explicitly. Equations 9.2, 14.1, and 14.2 have implicit forms, which can be quickly solved using standard math tools, such as Matlab. Multiple mathematical roots exist for these equations, but only one is physically correct. The following constraints should be imposed to determine the physically correct root:

1. h_f must be a non-negative real number.
2. The absolute value of pressure gradient m_2 and m_4 calculated based on the value of h_f must be non-negative.
3. Total penetration flow rate, $h_f V_\varepsilon$ must be smaller than the total inlet flow rate Q.

It is possible that none of mathematical roots is physically correct. This result occurs when the assumptions listed in the Modeling domain and assumptions section are not fully satisfied. For a negative capillary pressure case, if the coating speed is too high, the overall pressure in the coating bead, $p(x)$, might equal to or be smaller than p_{liquid}. In this case, the calculated h_f will be zero or negative. If h_f is zero, it means the $p(x)$ is balanced with p_{liquid}, thus no penetration occurs. If h_f is negative, it means that $p(x)$ is smaller than p_{liquid} and also no physical penetration occurs.

It has been assumed that the coating is conducted without defects (Assumption 7). However, the specific range of coating parameters, including Q, V, and H, to ensure a defect-free coating on a porous medium is beyond the scope of current study. As an approximation, the ranges of coating parameters were initially estimated based on analytical models for coating solid substrates,[25] and finally determined by experimental observation.

Experimental Validation

Materials and experimental design

Experiments have been conducted to validate the proposed analytical models for calculating penetration depth. Glycerin, a Newtonian fluid with 99.91 wt %, and blackstrap molasses, a non-Newtonian fluid, purchased of the shelf were used as test fluids. Glycerin has the following viscosity, density, and surface tension at room temperature: 0.91 Pa s,[26] 1260 kg/m^3, and 0.063 N/m,[27] respectively. Blackstrap molasses has the following power law properties, density, and surface tension at room temperature[28]: $m = 8.07$ Pa s^n, $n = 0.83$, 1452 kg/m^3, and 0.047 N/m, respectively.

The following die dimensions were fixed in experiments: $X_1 = 5.207$ mm, $X_2 = 4.648$ mm, $W = 250$ μm. The experiments were conducted at ambient temperature, 25°C. Three kinds of Toray carbon paper purchased from Toray Industries, Inc. were chosen as the porous media. Specifically, the carbon paper used in the experiments includes two batches of untreated TGP-H-090 and one batch of TGP-H-090 treated with 20% Polytetrafluoroethylene (PTFE). They were classified as TGP-H-090 (batch 1), TGP-H-090 (batch 2), and TGP-H-090 (PTFE), respectively.

The properties of the porous media are given in Table 1. Contact angle of two kinds of test fluids on the surface of the each carbon paper was measured in house by using a Rame–Hart goniometer. Measurements were conducted at least 10 times for each case and average values were calculated, as shown in Table 1. Due to the effect of penetration and the micropores structure on the surface of carbon paper, the measured contact angle has a relatively large deviation. Although, different lots of untreated TGP-H-090 are supposed to have the same properties, however, it was found that the contact angles for these two batches of untreated TGP-H-090 are different. Therefore, they were treated as two kinds of substrates in the experiments. The microstructure of Toray series carbon paper has been measured and studied extensively[29–33]; thus, it is assumed to be consistent for different batches. Therefore, other properties related with microstructure including permeability, porosity, and average pore radius are assumed to be consistent for different batches.

In this study, the capillary pressure in the porous media was calculated using Eq. 1, which is an approximate evaluation of the capillary effect in the porous media. The real capillary pressure is related with dynamic advancing contact angle and the microstructure inside the porous media,[21–24] which are far more complex and beyond the scope of the current study. The approximate values for capillary pressure for all cases are shown in Table 1. It can be seen that since

Table 2. Processing Parameters for Experiments

Test #	Substrate	Fluid	Flow rate, Q (mm^2/s)	Stand-off height, H (μm)	Coating speed range (mm/s)
1	TGP-H-090 (batch 1)	Molasses	0.520	140	2.3–5.8
2	TGP-H-090 (batch 1)	Molasses	0.288	140	1.5–3.6
3	TGP-H-090 (batch 1)	Molasses	0.715	250	2.2–4.7
4	TGP-H-090 (batch 2)	Molasses	0.848	170	4.0–5.6
5	TGP-H-090 (PTFE)	Molasses	0.848	170	3.6–5.3
6	TGP-H-090 (PTFE)	Molasses	1.143	210	4.8–5.2
7	TGP-H-090 (PTFE)	Molasses	0.730	170	3.2–4.0
8	TGP-H-090 (batch 1)	Glycerin	0.603	115	2.6–4.7
9	TGP-H-090 (batch 2)	Glycerin	0.706	130	3.6–5.2

all contact angles are higher than 90°, the capillary pressure values are all negative.

Experiments were conducted under different processing parameters as shown in Table 2. The roll-to-roll slot die coating system used in Ding et al's[6] earlier work was used in this study. The size of carbon paper samples was around 4×4 cm^2. The carbon paper samples were fixed on the surface of a polyethylene terephthalate (PET) film by sticking the edges with tape. PET film is the continuous moving substrate in the roll-to-roll slot die coating system. During the experiments, the flow from the slot die was continuous, while carbon paper samples were discontinuously fixed on the PET substrate and passed through the slot die. Before making each measurement, around 1 cm of carbon paper was cut from the four edges of the samples to avoid any edge effects. The coating speed was controlled to ensure no coating defects in the coating bead, such as air entrainment or pinholes.

Penetration depth measurement method

The penetration depth was determined by measuring the weight of the penetrated fluid. After coating the carbon paper, the top fluid on the coated sample was immediately and carefully removed with a blade. A schematic of the initial coated porous substrate is shown in Figure 4a; and Figure 4b shows the sample after the top fluid is removed. The total weight, M_t, and top surface area, A_t, of the sample without top fluid are measured first. Then the weight of the carbon paper, M_p, is calculated by $M_p = \rho_a \times A_t$, where ρ_a is the area density of the carbon paper. ρ_a has been measured to be around 1.186×10^{-4}, 1.264×10^{-4}, and 1.462×10^{-4} g/mm^2 for TGP-H-090 (batch 1), TGP-H-090 (batch 2), and TGP-H-090 (PTFE), respectively. The difference of the area density between the two batches of untreated TGP-H-090 corresponds to slight differences in thickness, which were measured to be around 180 and 195 μm for TGP-H-090 (batch 1) and TGP-H-090 (batch 2), respectively. The weight of the penetrated fluid, M_f, is calculated by $M_f = M_t - M_p$. Using M_f, the penetration depth is calculated by

$$h_f = \frac{M_f}{\rho A_t \varepsilon} \tag{19}$$

where ρ is the density of the coated liquid.

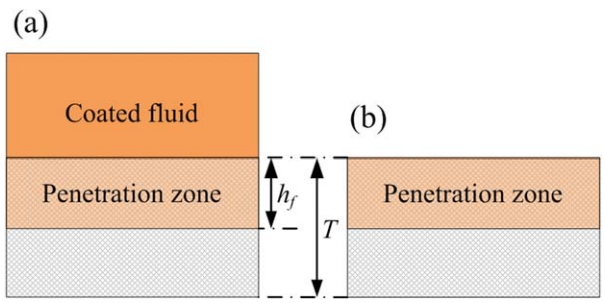

Figure 4. Schematic of coated porous substrate (a) with and (b) without the top fluid.

[Color figure can be viewed in the online issue, which is available at wileyonlinelibrary.com.]

Experimental results and discussion

The average penetration depth and standard deviation were obtained based on measuring three samples for each set of coating conditions. The experimental results of the nine tests are shown and compared with analytical results in Figures 5a–5h. It can be seen that the standard deviation of the measured penetration depth is generally smaller than ± 8 μm for all coating conditions; thus, the measurements are assumed to be repeatable. For comparison, the analytical penetration depth is calculated without considering capillary pressure, based on Ding et al.'s[14] previous models and considering the effect of a negative capillary pressure based on Equations 9.2 and 14.2 in this article. It can be seen from Figures 5a to 5h that the analytical models developed in this article agree with experimental results well, both qualitatively and quantitatively. The overall relative error between the predicted and measured penetration depth is generally lower than 20%. This agreement demonstrates that the developed models are relatively accurate.

As coating speed increases, the penetration depth decreases as would be expected. However, based on the tests, it was found that the penetration depth does not significantly decrease beyond 40 μm, which is approximately equivalent to twice of the average pore diameter. Physically this means that some pores on the surface of the carbon paper will be filled regardless of the coating velocity. Another reason for this lower limit of penetration depth is that some fluid might be driven into the carbon paper while the top layer of the fluid is being removed, before weighing the samples.

As it can be seen from Figure 5a, in Test #1, the capillary pressure does not significantly affect the penetration depth. The capillary pressure only shifts the curve of predicted penetration depth down by 5–10 μm. This small shift is because the maximum pressure in the coating bead for coating a solid substrate, which can be calculated by $\frac{6\bar{\mu}(2Q-VH)L_2}{H^3}$ based on Eq. 14.2, is between 8300 and 31,400 Pa, under the coating conditions of Test #1. This value is much higher than the absolute value of capillary pressure, 1500 Pa. Therefore, the pressure in the coating bead dominates fluid penetration. However, the maximum coating bead pressure is between 3000 and 17,400

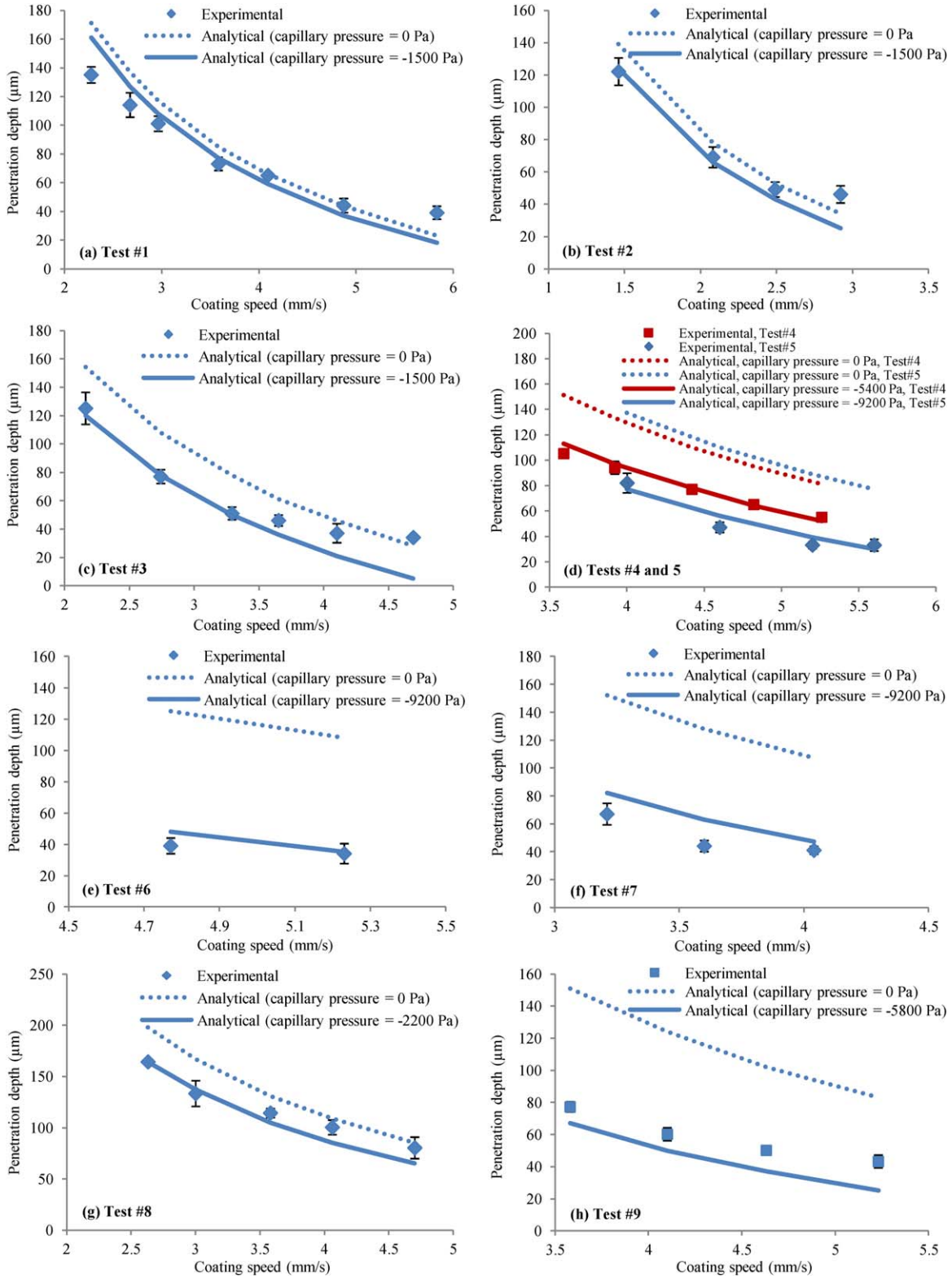

Figure 5. Experimental and predicted results of penetration depth.

[Color figure can be viewed in the online issue, which is available at wileyonlinelibrary.com.]

Pa in Test #2 and 1900–7600 in Test #3, which are much smaller than that in Test #1. Thus, the effect of capillary pressure is expected to be more significant in Tests #2 and #3. Comparing Figures 5b and c, it is shown that the capillary pressure shifts the curve of predicted penetration depth down by 9–15 and 23–34 μm for Tests #2 and #3, respectively, which is more significant than that observed in Test #1, as expected. Under coating conditions of Tests #2 and #3, the analytical model with capillary pressure gives a better prediction than that without capillary pressure.

Tests #4 and #5 were conducted using the same flow rate, stand-off height, and similar coating speed range but different substrates. One is TGP-H-090 (batch 2) the other is TGP-H-090 (PTFE). These two substrates have different permeability and porosity, and more importantly create different capillary pressure. Experimental results in Figure 5d clearly show the difference of penetration depth on these two substrates. Specifically, TGP-H-090 (PTFE) has a low penetration depth level because the PTFE-treated carbon paper is more hydrophobic, and thus has a tendency to push the fluid out of the pores. Compared with Tests #1, #2, and #3, the results in Figure 5d show an even more significant effect of capillary pressure on penetration depth. Specifically, the capillary pressure shifts the curve of predicted penetration depth down by 29–38 and 47–60 μm in Tests #4 and #5, respectively. Although the capillary pressure is higher, the developed models still give reasonable predictions for the penetration depth. The predicted values generally follow the same trend as the measured penetration depth. However, the error between the predicted and measured penetration depth is relatively larger for coating TGP-H-090 (PTFE), which is due to the uncertainties in the capillary pressure calculation and will be discussed in the Error Analysis section.

To double check the accuracy of the proposed models for relatively higher capillary pressure conditions, Tests #6 and #7 were conducted, using TGP-H-090 (PTFE). Different flow rates and coating speeds were used in these two tests. Results are shown in Figures 5e and f. Based on the results, the model that includes capillary pressure aligns better with the experimental results than the model that does not consider capillary pressure. The predicted penetration depth is reasonable and is in good agreement with experimental results. However, the error for a relatively higher capillary pressure condition; that is, -9200 Pa, in Tests # 5, #6, and #7, seems larger than the error for a relatively lower capillary condition; that is, -1500 Pa, in Tests #1 and #2 and -5400 Pa in Test #3. The error between predicted and measured penetration depth is affected by several uncertainty in the capillary pressure calculation, which will be analyzed in detail in the Error Analysis section.

Tests #8 and #9 were conducted by coating glycerin under different coating conditions. Two kinds of substrates were used: TGP-H-090 (batch 1) for Test #8 and TGP-H-090 (batch 2) for Test #9, respectively. Based on the results in Figures 5g and h, it can be seen that the predicted penetration depth matches the experimental results well. The general trend and error is similar to those for coating molasses. This means that the developed models give a reasonable prediction of penetration for both Newtonian and non-Newtonian fluids. However, the error between predicted and measured values in Test #9 seems larger than that in Test #8. This difference is believed to be related with the relatively higher capillary pressure in Test #9.

Validation of experimental conditions

The power law model of the viscosity for non-Newtonian molasses measured by Bhamidipati et al.[28] is generally valid for a shear rate between 1 and 100 1/s. In this study, the shear rate of porous flow can be approximately evaluated by $v_{\text{p-ave}}/r$, where $v_{\text{p-ave}}$ is the average penetration velocity and r is the average pore radius. $v_{\text{p-ave}}$ can be approximated by $h_{\text{f}}/(L_2/V)$, where the denominator is the approximate penetration time. For the flow in the coating bead, the shear rate can be approximated by V/H. Using the data from Tests #1 to #7, the shear rate is 3–9 and 10–40 1/s for the porous flow and the flow in the coating bead, respectively. Therefore, the power law model of Molasses measured by Bhamidipati et al.[28] is valid for the coating conditions in this study.

As discussed above, the generalized lubrication theory, Eqs. 14.1 and 14.2, used in the analytical modeling of penetration depth for non-Newtonian fluids can give a relatively good approximation for the pressure gradient when the flow behavior index, n, is higher than 0.5 and the flow rate in the channel is between $0.2VH$ and $0.8VH$.[15] In this study, the flow behavior index of Molasses is 0.83. The approximate flow rate in the right channel, $Q-h_{\text{f}}V\varepsilon$, is $0.3VH-1.0VH$, which is close to the range required for a good approximation, but, may be outside the boundary. Therefore, the developed analytical penetration depth models for non-Newtonian fluids can be approximately used for the coating conditions in current study.

Error analysis

Based on previous experimental results, it seems that the error between the predicted and measured penetration directly depends on the magnitude of the capillary pressure. Higher capillary pressure seems to generate larger error. This association is because of several uncertainties in the capillary pressure calculation. One uncertainty is caused by the average pore radius used in Eq. 1. The pore radius of Toray series carbon paper has been extensively studied by many researchers using different methods. The most common method used is mercury intrusion porosimetry,[29,31,34,35] in which the carbon paper is assumed to be composed of a bundle of capillary tubes, and the pore radius is the radius of the capillary tubes. Other methods that have been used to study the pore radius of Toray series carbon paper include the method of standard porosimetry,[30] confocal microscopy,[36] pore network model,[33] and the breakthrough pressure of water.[37] There are inconsistencies in the results of different investigations, but the typical value of the average pore radius in Toray series carbon paper has been found to be around 10 μm.[38] The values shown in Table 1 were selected to be close to the typical value, which introduces error into the capillary pressure calculation.

Another uncertainty related to the capillary pressure calculation comes from the contact angle measurement. There are several contact-angle concepts related to porous media. The contact angle observed on the surface of a porous medium is usually referred as an apparent contact angle; whereas the contact angle on the chemically heterogeneous fibers is usually referred as an effective contact angle.[30] The Cassie–Baxter equation can be used to evaluate the effective contact angle based on the apparent contact angle[39]; however, the Cassie–Baxter equation is derived based on a grid formed of cylindrical fibers, which is not the case for carbon paper in this study. The contact angle measured in current study is a static contact angle; while the contact angle during the penetration process is dynamic[21,23] and expected to be advancing. Therefore, the capillary pressure in the porous media should be governed by an effective-advancing contact angle, vs. an apparent-static contact angle. Since an effective contact angle is usually smaller than an apparent contact angle,[30,39] but an advancing contact angle is larger than a static contact angle, it is very difficult to compare the relative magnitude

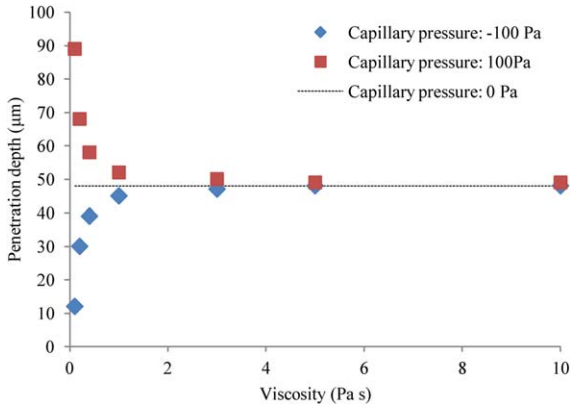

Figure 6. Effect of viscosity and capillary pressure on the penetration depth.

[Color figure can be viewed in the online issue, which is available at wileyonlinelibrary.com.]

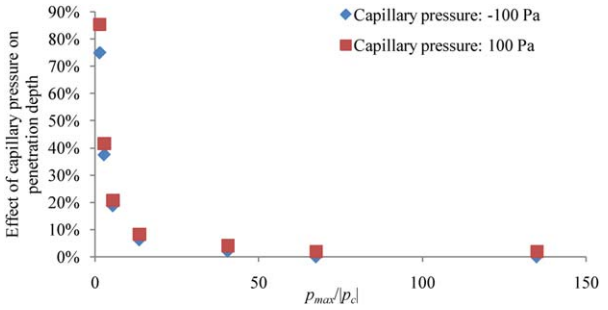

Figure 7. Relationship between $\frac{p_{max}}{|p_c|}$ and the effect of capillary pressure on penetration depth.

[Color figure can be viewed in the online issue, which is available at wileyonlinelibrary.com.]

between an effective-advancing contact angle and an apparent-static contact angle. In addition, due to the effect of penetration and the microporous structure on the surface of carbon paper, the measured contact angle in this study has a relatively large deviation, as shown in Table 1. Thus, the uncertainty of the contact angle is expected to introduce error into the capillary pressure calculation.

Except the error introduced by approximating the capillary pressure, other error sources include the approximations and simplifications used when developing the models, and the instability or uncertainty of the coating speed, flow rate, stand-off height, and porous media properties used in the experiments. Considering all of these effects, it is believed that the experimental results shown in Figures 5a–h are reasonable, and can serve as evidence that the analytical models developed in this study are relatively accurate.

Effects of viscosity and capillary pressure on penetration depth

The effects of coating speed, flow rate, permeability, and porosity on penetration depth during slot die coating have been discussed in detail by Ding et al.[14] In this article, the effects of viscosity and capillary pressure on penetration depth are investigated using the models, previously discussed. Specifically, the capillary pressure is fixed as 100 and -100 Pa, viscosity changes from 0.1 to 10 Pa s, while all other coating conditions include: $V=3.5$ mm/s, $Q=1$ mm^2/s, $k=9.375\times10^{-13}$ m^2, $\varepsilon=0.75$, $X_2=3$ mm, $W=250$ μm, $H=250$ μm. The penetration depths calculated using different capillary pressure and viscosity values are shown in Figure 6.

As shown in Figure 6, when the capillary pressure is negative the penetration depth increases as viscosity increases; whereas when capillary pressure is positive the penetration depth decreases as viscosity increases. With increasing viscosity, the penetration depth, regardless of the capillary pressure, approaches 48 μm, which is the value obtained with zero capillary pressure. This result suggests that at a lower viscosity the capillary pressure has a more significant effect on the penetration depth; and vice versa. This result is reasonable because the penetration depth is governed by both the pressure in the coating bead and the capillary pressure in the porous media. If the viscosity is low, the capillary pressure will dominate the penetration; while if the viscosity is sufficiently high, the pressure in the coating bead will dominate the penetration and the penetration depth approaches a constant value. In order to evaluate the relative importance of the coating bead pressure and the capillary pressure, the dimensionless value $\frac{p_{max}}{|p_c|}$ is evaluated, where p_{max} is the maximum coating bead pressure of coating a solid substrate. Based on Eqs. 5.2 and 14.2, $\frac{p_{max}}{|p_c|}$ can be given as

$$\frac{p_{max}}{|p_c|}=\frac{6\mu(2Q-VH)L_2}{H^3|p_c|} \quad \text{(Newtonian fluids)} \qquad (20.1)$$

$$\frac{p_{max}}{|p_c|}=\frac{6\bar{\mu}(2Q-VH)L_2}{H^3|p_c|} \quad \text{(non-Newtonian fluids)} \qquad (20.2)$$

The effect of capillary pressure on penetration depth in Figure 6 can also be evaluated by $\left|\frac{h_{fc}-h_{fo}}{h}\right|\times100\%$, which is the absolute percentage difference between the penetration depth calculated with capillary pressure, h_{fc}, and that calculated without capillary pressure, h_{fo}. The relationship between $\frac{p_{max}}{|p_c|}$ and the effect of capillary pressure on penetration depth is shown in Figure 7. It can be seen that the effect of capillary pressure on penetration depth is less than 10% when $\frac{p_{max}}{|p_c|}$ is higher than 10. Therefore, $\frac{p_{max}}{|p_c|}=10$ may be used as a criterion to determine whether the effect of capillary pressure on penetration depth is significant.

Penetration during the phase transition process beyond the slot die

The results in Figure 6 suggest that the capillary effect on the penetration depth can be ignored if the fluid viscosity is sufficiently high. Therefore, the change of penetration depth beyond the die can be ignored for a high viscosity fluid. This conclusion is expected to be valid for other coating processes, such as blade coating and roll coating, although the models developed here are only for slot die coating. Indeed, Yesilalan et al.[7] showed that viscosity had no effect on penetration depth in a blade coating process. Their observation is attributed to the high viscosity (36.7, 98.8, and 158 Pa s) of the fluids used in their experiments.

Another factor that prevents the change of penetration depth beyond the slot die is the pinning effect, which is related to two-phase flow in random fiber porous media.[24] Wiklund and Uesaka[24] used a free-energy lattice Boltzmann approach to perform simulations of liquid penetration into random porous media. Their results showed that the liquid front stops and the line of contact can be pinned by surface roughness or discontinuities on the solid-surface, including

sharp edges, high-curvature points, widening pores, and branching channels. They found that penetration driven by capillary pressure cannot consistently continue due to pinning.

Though the change of penetration depth during the phase transition region is complex to model due to the uncertainty of material properties, we still can expect that the penetration depth may not change much beyond the slot die due to the relatively high viscosity of the fluids considered and the pinning effect. This suggests that the model developed to calculate the final penetration depth under the coating bead, in this study, can be directly used to evaluate the overall penetration depth under following assumptions:

1. Viscosity of coating fluids is sufficiently high, thus capillary effect can be ignored, and

2. Porous medium has a random microstructure, thus there are pinning effects in the porous media.

Conclusions

A series of analytical models of penetration depth during slot die coating on porous media were developed for both Newtonian and non-Newtonian fluids, with the effect of capillary pressure considered. Experiments of coating Newtonian glycerin and non-Newtonian blackstrap molasses onto Toray series carbon paper were conducted to validate the developed models. The overall relative error between the predicted and measured penetration depth was generally lower than 20%. This demonstrates that the developed models are relatively accurate. It was also found that a higher capillary pressure introduces increased error to the analytical models. A parametric study showed that at a lower viscosity the capillary pressure has a more significant effect on the penetration depth; and vice versa. If the viscosity is high enough, the effect of capillary pressure will be negligible and the penetration depth approaches a constant value. $\frac{p_{\max}}{|p_c|}=10$ calculated using Eqs. 20.1 and 20.2 can be used as an approximate criterion to determine whether the effect of capillary pressure on penetration depth is significant. The penetration depth may not change much beyond the slot die due to high viscous effect and pinning effects.

Acknowledgment

This work was supported by the National Science Foundation under grant number 0928093.

Notation

A_t = area of a carbon paper sample
h = penetration depth
h_0 = penetration depth at $x=0$
h_f = final penetration depth at the outlet
h_{fc} = penetration depth calculated with capillary pressure
h_{fo} = penetration depth calculated without capillary pressure
H = stand-off height
k = permeability of porous media
L_1 = left channel length
L_2 = right channel length
m = consistency index of apparent viscosity of a non-Newtonian fluid
m_1 = pressure gradient in the left channel for coating a Newtonian fluid
m_2 = pressure gradient in the right channel for coating a Newtonian fluid
m_3 = pressure gradient in the left channel for coating a non-Newtonian fluid
m_4 = pressure gradient in the right channel for coating a non-Newtonian fluid
n = flow behavior index of apparent viscosity of a non-Newtonian fluid
p = pressure
p_{air} = reference pressure of air
p_c = capillary pressure
p_{liquid} = pressure at the front of penetrated fluid
p_{max} = maximum coating bead pressure of coating a solid substrate
q_1 = flow rate in left channel
q_2 = flow rate in the right channel
Q = inlet volumetric flow rate of slot coating
r = average pore radius
v_p = penetration velocity
$v_{p\text{-}ave}$ = average penetration velocity
V = coating speed
W = slot width
x = coordinate along the coating direction
X_1 = left die lip length
X_2 = right die lip length
y = coordinate vertical to the coating direction
A, B, and C = variables defined in analytical expressions of final penetration depth
M_t, M_f, and M_p = weight variables defined in the measurement of penetration depth
s_1, s_2, s_3, and s_4 = position variables defined in derivation of penetration depth for a negative capillary pressure

Greek letters

ε = porosity of porous media
μ = viscosity of a Newtonian fluid
μ_{app} = apparent viscosity of a non-Newtonian fluid
μ_{eff} = effective viscosity defined in Blake–Kozeny equation
$\bar{\mu}$ = viscosity term defined in non-Newtonian lubrication equation
ρ = fluid density
ρ_a = area density of carbon paper
σ = surface tension
θ = contact angle of coating fluid on the surface of porous media

Literature Cited

1. Park Y, Kim E. Wearing comfort of temperature-adaptable textiles by dual-phase coatings between phase-change materials and silicon carbide particles. *J Appl Polym Sci*. 2012;126:E151–E158.
2. Meng QB, Lee S-I, Nah C, Lee Y-S. Preparation of waterborne polyurethanes using an amphiphilic diol for breathable waterproof textile coatings. *Prog Org Coat*. 2009;66:382–386.
3. Didane N, Giraud S, Devaux E. Fire performances comparison of back coating and melt spinning approaches for PET covering textiles. *Polym Degrad Stab*. 2012;97:1083–1089.
4. Bashir T, Skrifvars M, Persson NK. Surface modification of conductive PEDOT coated textile yarns with silicone resin. *Mater Technol*. 2011;26:135–139.
5. Ding X, Didari S, Fuller TF, Harris TA. A new fabrication technique to manufacture an MEA using direct coating of Nafion onto catalyzed GDL. *ECS Trans*. 2010;33:255–265.
6. Ding X, Didari S, Fuller TF, Harris TAL. Membrane electrode assembly fabrication process for directly coating catalyzed gas diffusion layers. *J Electrochem Soc*. 2012;159:B746–B753.
7. Yesilalan HE, Warner SB, Laoulache R. Penetration of blade-applied viscous coatings into yarns in a woven fabric. *Text Res J*. 2010;80:1930–1941.
8. Li Y, He B. Characterization of ink pigment penetration and distribution related to surface topography of paper using confocal laser scanning microscopy. *BioResources*. 2011;6:2690–2702.
9. Matilainen K, Hamalainen T, Savolainen A, et al. Performance and penetration of laccase and ABTS inks on various printing substrates. *Colloids Surf B: Biointerfaces*. 2012;90:119–128.
10. Letzelter P, Eklund D. Coating color dewatering in blade coaters—part 1: mathematical model and the influence of color parameters. *Tappi J*. 1993;76:63–68.
11. Chen KSA, Scriven LE. Liquid penetration into a deformable porous substrate. *Tappi J*. 1990;73:151–161.

12. Ninness B, Bousfield DW, Triantafillopoulos NG. Fluid dynamics model of the film-fed rolling nip with a porous web. Coating/Papermakers Conference; May 4–6, 1998;New Orleans.
13. Devisetti SK, Bousfield DW. Fluid absorption during forward roll coating of porous webs. *Chem Eng Sci*. 2010;65:3528–3537.
14. Ding X, Fuller TF, Harris TAL. Predicting fluid penetration during slot coating onto porous substrates. *Chem Eng Sci*. 2013;99:67–75.
15. Dien IK, Elrod HG. A generalized steady-state reynolds equation for non-Newtonian fluids, with application to journal bearings. *ASME J Tribol*. 1983;105:385–390.
16. Christopher RH, Middleman S. Power-law flow through a packed tube. *Ind Eng Chem Fundam*. 1965;4:422–426.
17. Savins JG. Non-newtonian flow through porous media. *Ind Eng Chem*. 1969;61:18–47.
18. Ghassemzadeh J, Hashemi M, Sartor L, Sahimi M. Pore network simulation of imbibition into paper during coating: I. *model development*. *AIChE J*. 2001;47:519–535.
19. Letzelter P, Eklund D. Coating color dewatering in blade coaters—part 2: the influence of machine configuration. *Tappi J*. 1993;76:93–98.
20. Ghassemzadeh J, Sahimi M. Pore network simulation of fluid imbibition into paper during coating—III: modeling of the two-phase flow. *Chem Eng Sci*. 2004;59:2281–2296.
21. Marmur A. Kinetics of penetration into uniform porous media: Testing the equivalent-capillary concept. *Langmuir*. 2003;19:5956–5959.
22. Marmur A, Cohen RD. Characterization of porous media by the kinetics of liquid penetration: the vertical capillaries model. *J Colloid Interface Sci*. 1997;189:299–304.
23. Lavi B, Marmur A, Bachmann J. Porous media characterization by the two-liquid method: effect of dynamic contact angle and inertia. *Langmuir*. 2008;24:1918–1923.
24. Wiklund HS, Uesaka T. Microfluidics of imbibition in random porous media. *Phys Rev E*. 2013;87:023006.
25. Higgins BG, Scriven LE. Capillary pressure and viscous pressure drop set bounds on coating bead operability. *Chem Eng Sci*. 1980; 35:673–682.
26. Sheely ML. Glycerol viscosity tables. *Ind Eng Chem*. 1932;24:1060–1064.
27. Cheng P, Li D, Boruvka L, Rotenberg Y, Neumann AW. Automation of axisymmetric drop shape analysis for measurements of interfacial tensions and contact angles. *Colloids Surf*. 1990;43:151–167.
28. Bhamidipati KL, Didari S, Bedell P, Harris TAL. Wetting phenomena during processing of high-viscosity shear-thinning fluid. *J Nonnewton Fluid Mech*. 2011;166:723–733.
29. Tamayo A, McGregor F, Bahrami M. Single phase through-plane permeability of carbon paper gas diffusion layers. *J Power Sources*. 2012;204:94–99.
30. Gostick JT, Fowler MW, Ioannidis MA, Pritzker MD, Volfkovich YM, Sakars A. Capillary pressure and hydrophilic porosity in gas diffusion layers for polymer electrolyte fuel cells. *J Power Sources*. 2006;156:375–387.
31. Lobato J, Cañizares P, Rodrigo MA, Ruiz-López C, Linares JJ. Influence of the teflon loading in the gas diffusion layer of PBI-based PEM fuel cells. *J Appl Electrochem*. 2008;38:793–802.
32. Flückiger R, Freunberger SA, Kramer D, Wokaun A, Scherer GG, Büchi FN. Anisotropic, effective diffusivity of porous gas diffusion layer materials of PEFC. *Electrochim Acta*. 2008;54:551–559.
33. Gostick JT, Ioannidis MA, Fowler MW, Pritzker MD. Pore network modeling of fibrous gas diffusion layers for polymer electrolyte membrane fuel cells. *J Power Sources*. 2007;173:277–290.
34. Williams MV, Begg E, Bonville L, Kunz HR, Fenton JM. Characterization of gas diffusion layers for PEMFC. *J Electrochem Soc*. 2004; 151:A1173–A1180.
35. Fairweather JD, Cheung P, Schwartz DT. The effects of wetproofing on the capillary properties of proton exchange membrane fuel cell gas diffusion layers. *J Power Sources*. 2010;195:787–793.
36. Gao B, Steenhuis TS, Zevi Y, Parlange J-Y, Carter RN, Trabold TA. Visualization of unstable water flow in a fuel cell gas diffusion layer. *J Power Sources*. 2009;190:493–498.
37. Benziger J, Nehlsen J, Blackwell D, Brennan T, Itescu J. Water flow in the gas diffusion layer of PEM fuel cells. *J Membr Sci*. 2005;261: 98–106.
38. Fishman Z, Hinebaugh J, Bazylak A. Microscale tomography investigations of heterogeneous porosity distributions of PEMFC GDLs. *J Electrochem Soc*. 2010;157:B1643–B1650.
39. Cassie ABD, Baxter S. Wettability of porous surfaces. *Faraday Soc Trans*. 1944;40:546–551.

Manuscript received Apr. 13, 2014, and revision received July 15, 2014.